

The YMDB catalog: Young massive detached binaries for the determination of high-precision absolute stellar parameters*

Pablo Martín-Ravelo^{1,2}, Roberto Gamen^{3,4}, Julia I. Arias¹, André-Nicolas Chené², and Rodolfo H. Barbá ^{**1}

¹ Departamento de Astronomía, Universidad de La Serena, Av. Cisternas 1200 Norte, La Serena, Chile.

² Gemini Observatory/NSF's NOIRLab, 670 N. A'ohoku Place, Hilo, HI 96720, USA
e-mail: pablo.martin@noirlab.edu

³ Instituto de Astrofísica de La Plata, CONICET–UNLP, Paseo del Bosque s/n, 1900, La Plata, Argentina.

⁴ Facultad de Ciencias Astronómicas y Geofísicas, Universidad Nacional de La Plata, Argentina.

Received: 20 June 2024 / Accepted: 05 July 2024

ABSTRACT

Context. Massive stars play a crucial role in the cosmic dynamics and chemical evolution of galaxies. Despite their significance, our understanding of their evolution and properties remains limited. An accurate determination of stellar parameters, such as the mass and radius, is essential for advancing our knowledge. Detached eclipsing binaries (DEBs) are particularly valuable for these determinations due to the minimal interaction between their stellar components, allowing for precise measurements.

Aims. This study aims to introduce the Young Massive Detached Binary (YMDB) catalog, designed to address the gap in the high-precision absolute parameter determination for young massive stars. By focusing on DEBs within the spectral range O9–B1, this catalog seeks to provide a reliable database for future astronomical studies and improve our understanding of massive star evolution.

Methods. We conducted a photometric analysis of 87 young massive stars in detached eclipsing systems using TESS light curves (LCs) that were processed through a custom pipeline. This analysis involved determining the amplitude of magnitude variations, orbital periods, times of minima, eccentricities, and the presence of apsidal motion and heartbeat phenomena. A thorough literature review was performed to obtain MK spectral classifications. We performed our own spectral classification of 19 systems to support the sample where a new classification was lacking or inconclusive.

Results. The analysis identified 20 previously unreported binary systems, with 13 newly recognized as variable stars. Among the 87 stars examined, 30 are confirmed as YMDB members, and 25 are candidates pending spectral classification. The exclusion of the remaining 32 stars is attributed to unsuitable spectral types or their nondetached binary nature. Notable findings include the identification of new LC classifications, eccentricities in 13 systems, and heartbeat phenomena in several targets.

Conclusions. The YMDB catalog offers a resource of high-quality LCs and reliable stellar classifications, serving as a valuable tool for the astronomical community.

Key words. stars: fundamental parameters – stars: binaries: eclipsing – stars: binaries: spectroscopic – stars: early-type – stars: massive – catalogs

1. Introduction

Massive stars, defined by their cataclysmic end as core collapse supernovas, are typically those with an initial mass of eight or more solar masses and they fall into the OB spectral classification. These stellar behemoths play a crucial role in cosmic dynamics and chemical evolution, with their supernova events significantly enriching the interstellar medium with heavy elements. Understanding massive stars is fundamental to comprehending stellar evolution, the evolutionary history of galaxies, and the Universe at large. Due to their immense luminosity, they are key observable objects in distant galaxies, making them essential for astronomical studies with both current and forthcoming space and ground-based large telescopes.

Our current understanding of massive star evolution remains limited, as evidenced by the persistent mass discrepancy be-

tween empirical measurements from orbital dynamics and theoretical model predictions. This discrepancy has been a long-standing issue in astrophysics (see e.g., [Herrero et al. 1992](#); [Weidner & Vink 2010](#), and references therein). Factors inherent in binary systems, such as stellar rotation, which influence orbital ellipticity, synchronization, tidal effects, limb darkening, and radiative propagation, are crucial in this context. Evolutionary models that incorporate rotation show marked differences compared to nonrotational models. Additionally, research by [Martins & Palacios \(2013\)](#) highlights significant variations in how current models handle mass loss in these stars.

The determination of reliable masses for massive stars is only achievable in binary systems, particularly through the study of light curves (LCs) and radial velocity (RV) curves of eclipsing binaries. The likelihood of encountering massive stars within binary systems is fairly high, especially during their main sequence phase, the most extended period of a star's lifecycle. Comprehensive spectroscopic surveys reveal that around 75% of main sequence O-type stars (cf. [Barbá et al. 2017](#)), and a similar

* Full version of Tables 2, 3 and 4 are only available in electronic form at the CDS via anonymous ftp to cdsarc.u-strasbg.fr (130.79.128.5) or via <http://cdsweb.u-strasbg.fr/cgi-bin/qcat?J/A+A/>.

** In Memoriam (1962–2021)

ratio of early B-type stars (Chini et al. 2012), are part of gravitationally bound systems.

The endemic multiplicity among massive stars offers unique research opportunities, although the method has its limitations. An inherent consequence of binarity is the interaction among its components, which make their evolution paths deviate from those of solitary stars of similar types. This interaction issue was emphasized by Sana et al. (2012), who found that at least 71% of O-type stars in binary systems interact with their companions during their lifetimes, with 29% eventually merging into a single entity. Detecting past interactions poses challenges, as evidenced by discrepancies between empirical mass measurements and predictions from atmospheric or stellar evolution models, which often overlook these interactions.

Detached eclipsing binaries (DEBs) stand as critical objects in this context. These systems, characterized by a negligible or minimal interaction between their stellar components, perfectly meet the criteria for accurate stellar analysis. Given that most massive stars are part of multiple systems, it is preferable to focus on those with well-documented multiplicity. The best single stars for study are often the components of binary systems, as proposed by de Mink et al. (2011) and further discussed by Ekström (2021). DEBs provide a unique opportunity to determine the physical properties of stars with a high accuracy, such as their masses, and radii. Moreover, they can be used to determine distances. In this context, DEBs are key objects. Determinations from DEBs form the basis for calibrating crucial relationships among stellar parameters, such as the mass–luminosity relationship.

Among massive stars, those within the O8–B3 spectral-type range are predominant (just as a consequence of the stellar mass distribution). However, only a limited number have had their absolute parameters accurately determined. Our research aims to address this gap by examining a selection of DEBs within this spectral range. We intend to analyze their LCs and RV curves to derive precise stellar parameters.

In this work, we present a curated database of young massive stars, with spectral types around B0 V, in DEBs. This endeavor is the first step to maintain an up-to-date database of empirical absolute parameters for massive stars. To achieve our objectives, we have carefully selected systems from a careful search in the available literature (see details in Sect. 2.1). After that, we generated the LCs of each target in the database using data from the NASA Transiting Exoplanet Survey Satellite (TESS), and analyzed their variations to identify DEBs. This is explained in Sect. 2.2. TESS LCs were also examined for periodicities, to determine eccentricities, ephemerides, and also for the detection of pulsation and/or heartbeat phenomena. Some targets were spectroscopically observed to obtain their spectral classification, which were confusing in the literature. Observations are described in Sect. 2.4. All of the results that populate the Young Massive Detached Binaries (YMDB) catalog are shown in Sect. 3.

2. General methodology for the YMDB catalog

Our study's approach integrates a thorough search and analysis methodology to identify and evaluate candidates for detailed investigation. Starting with an extensive review of databases and literature, we refined our list of potential candidates by examining their spectral classifications and the likelihood of misclassification, and by quickly reviewing raw TESS LCs to exclude any undoubted nondetached binaries. This process narrowed our initial pool to 87 candidates.

In preparing the LCs, we initially set up background and target masks using a structured pixel grid to minimize light contamination, which is vital for precise LC extraction. We continuously evaluated data quality and implemented polynomial fitting to correct known and recurrent flux pattern variations in the TESS data, such as rollovers, ensuring a cleaner and more accurate representation of the LCs.

We utilized Gaussian Fitting (GF) and Box Least Square (BLS) methods to accurately determine orbital periods and other temporal features. Further analysis of the LCs involved meticulous visual inspection to confirm the detached nature of systems and identify any additional features such as pulsations or heartbeats.

To enhance the validity of the spectral classifications, new spectroscopic observations were conducted using the Jorge Sánchez telescope at CASLEO. These efforts were focused on acquiring low-resolution spectra, which were processed using established methods, to clarify any existing classification uncertainties.

2.1. Candidates selection

Candidates for the study were identified through extensive searches in various databases and literature. These sources included the Spectroscopic Binary Orbits Ninth Catalog (Pourbaix et al. 2004), OWN Survey (Gamen et al. 2007, 2008; Barbá et al. 2017), IACOB (Simón-Díaz et al. 2011), Eclipsing Variables Catalog (Avvakumova et al. 2013), and the multiplicity of northern O-type spectroscopic systems project (MONOS; Maíz Apellániz et al. 2019b; Trigueros Páez et al. 2021), among others. Additionally, potential targets suggested by collaborative efforts within the astronomical community were also considered.

The search criteria encompassed a wide range, including systems with components in the O7–B3 III–V spectral class, to account for potential misclassifications. This cautious approach was used to ensure all potentially relevant systems were considered, particularly those that might align with the desired O9–B1 IV–V classification upon closer scrutiny. A thorough review of the bibliography was conducted to assess the reliability of the spectral classifications, the availability of LCs, and the reported detachment status in the literature, narrowing down the original list of 339 targets to 186 candidates.

The process continued with an analysis of TESS data to eliminate any candidates showing clear non-Algol type variability (i.e. Beta Lyrae and W Ursae Majoris) reducing the number to 114 candidates. A custom pipeline was then developed for extracting high quality TESS LCs, allowing for the estimation of orbital periods (P) and minima (T0), as well as the identification of eccentric orbits, heartbeats and apsidal motion throughout the TESS sectors. This was achieved using both GF and BLS methods. The candidates were meticulously scrutinized, focusing on the identification of Algol-type variables. Systems not fitting the Algol type criteria were excluded, resulting in 87 stars qualifying as potential candidates which we present in this work. Details of this task are given in the following.

2.2. Construction of light curves

In constructing the LC, the initial step involved assessing the quality masks for each TESS sector, related to the star, to determine whether the default rejection criteria were adequate. For the majority of LCs, it was found that the default quality mask met the needs effectively.

2.2.1. Background mask

To construct a sky background mask for each sector, a 30×30 pixel area centered on the target system is analyzed. Stars within this area, along with their magnitudes, are identified using Gaia DR3 data. The `LIGHTKURVE` tool (Lightkurve Collaboration et al. 2018) is then employed to generate a mask with threshold zero, specifically excluding pixels affected by stars brighter than a determined magnitude limit. This upper limit is set at 5 magnitudes fainter than the brightest star within a 3-pixel radius of the target system, effectively minimizing contamination from other stars in the extraction of the desired LC.

2.2.2. Target mask

Following the construction of the sky background mask, a target mask is developed using a similar methodology. The function that delineates boxes around mapped stars based on their brightness is also applied to isolate the Target Pixel File (TPF) surrounding the star of interest. Adjustments to the size and position of this cut, alongside a specified threshold value, are made using the `LIGHTKURVE` tool to craft the target mask. This stage might require iteration, involving comparisons of the resulting LC with published ones and the LCs of individual pixels, to verify the accuracy of the selected parameters and the suitability of the target mask.

2.2.3. Data selection

The analysis of the unfolded extracted LC involves identifying and flagging problematic data that could compromise the construction of the LC. A visual inspection of the cadence for each TESS sector is essential, as it can reveal areas potentially affected by gaps in data—either due to TESS CCD readouts or data omitted by the quality mask. Data adjacent to these gaps might exhibit a different background profile, making parts of the LC unreliable if the background extraction fails to account for this variance. Additionally, these segments may experience slight magnitude shifts (Δmag) and may require independent normalization, posing challenges for systems with long periods.

2.2.4. Determination of ephemeris

In determining the ephemeris of our studied systems, we incorporate two principal methods: GF and BLS. GF is primarily utilized for its simplicity and effectiveness in identifying eclipse minima by fitting Gaussian profiles, a method similar to the Phase Dispersion Minimization (PDM) approach.

Phase dispersion minimization is traditionally used to detect stable periodic signals by minimizing scatter across phased data, making it ideal for datasets like those from TESS which may include gaps or nonsinusoidal variations. By adapting this methodology, our GF process not only identifies the minima but also estimates the period from these minima's separations, similarly to how PDM assesses periodicity by examining the variance across different data bins.

After initial minima identification, we fold the LC and apply GF iteratively across all sectors, optimizing the ephemeris precision in a manner analogous to refining PDM's phase coverage by adjusting bin overlaps or employing smoother functions in updated PDM versions.

Box least square is used alongside GF for period verification, with both methods critically reviewed against known periods from literature when available in order to cross-verify with es-

tablished data the reliability of our adapted PDM-inspired techniques in analyzing TESS's time series data.

2.2.5. Phase-synchronized polynomial fitting

Photometric observations from the TESS mission, similar to those from its predecessor Kepler, are susceptible to instrumental systematic trends that can obscure or distort the intrinsic stellar signals. These systematics arise primarily from spacecraft jitter and other operational imperfections, which introduce noise and trends across different timescales into the captured LCs.

To mitigate these effects, we employed a polynomial fitting method, analogous to the Pixel Level Decorrelation (PLD) method utilized in the EVEREST pipeline for K2 data. This method has been demonstrated to effectively remove correlated noise due to spacecraft motion by fitting and subtracting systematics directly from the pixel-level data (Luger et al. 2016).

While our approach uses a simpler polynomial fitting of lower orders, it shares the core principle of modeling the observed data to isolate and remove instrumental signatures. The primary distinction of our method, which we designate as "Phase-Synchronized Polynomial Fitting" (PSPF), lies in its utilization of the previously known orbital periods to synchronize (fold) phase points within a TESS sector. This synchronization enables the calculation of fits for data points that share the same phase, thus forming a more complex function that better adapts to the unique signal trends of TESS data. Therefore, PSPF is suited for systems with orbital periods shorter than the duration of a TESS sector. The method cannot be applied if the period exceeds the sector length (PLD should be used in those cases), unless the signal is expected to remain constant in different phases of the LC, such as outside the eclipses in highly detached binaries. It becomes particularly reliable when the orbital period is substantially shorter than the sector length, allowing for enhanced signal integrity post-correction through multiple phase folds.

The correction process begins with the identification of phase points across the LC that are consistent over multiple orbits, meaning without flux variations other than those related to the eclipsing nature of the system or other synchronized pulsations (whose periods are multiple of the orbital period). This leverages the comparative stability of shorter-period systems which may ignore not-synchronized variations if enough points per phase are provided. Each phase point will provide then a value not only for that phase, but for every other phase point in the LC. A weighted mean is calculated for these values in each phase point to construct a robust fit model. This model is then used to adjust the LC, with the median of all polynomial corrections applied to derive the final corrected LC. This procedure was only implemented when a consistent pattern of systematic error was evident across the entire sector, ensuring that the corrections made were both meaningful and substantiated by the data.

For about 20% of the candidates in our study that exhibited clear systematic trends, the PSPF was crucial for assembling a clean LC. A polynomial fit of order 1 was mainly used, but the selection of polynomial order was tailored to each target's specific noise characteristics, with higher orders only used seldom and for more complex systematic patterns.

Our PSPF corrections were validated against already corrected LCs, showing a significant reduction in noise and the preservation of intrinsic astrophysical signals and effectively detrending the TESS LCs, akin to the results reported by the EVEREST pipeline when applying PLD to K2 data (Luger et al. 2018).

2.3. Light-curves analysis

All generated LCs underwent meticulous inspection to confirm their detached nature, identify any pulsations or heartbeats, and determine eccentricity and apsidal motion. Visual inspection was used to confirm the detached nature of the system, which was unequivocally determined by the distinct transitions marking the beginning and end of eclipses in the LC. Pulsational features, indicative of either intrinsic variability of the components or the presence of a complex multiple system, were also identified through visual inspection of the LCs. In cases of multiple systems, efforts were made to disentangle the LCs using templates crafted from median data selected, when possible, from segments of the LC minimally affected by eclipses or intrinsic pulsations of the main system. The heartbeat phenomenon was identified as a distinct photometric variation occurring during orbital phases with closer eclipses, indicative of the expected periastron. We compared those variations against all forms of heartbeat showed in [Thompson et al. \(2012\)](#). Detailed descriptions of these cases are provided in Section 3.3 and their LCs are shown in Figure 6.

For systems where eccentricity was not immediately obvious, we employed GF to precisely measure the centers of the primary and secondary eclipses, using a threshold of $\Delta\phi=0.0002$, to determine whether their phase separation differed from 0.5. It is important to note that an exact half-period interval between eclipses does not necessarily imply a circular orbit; the system could be eccentric with a periastron longitude of either 90° or 270° . Therefore, values listed in Tables 2, 3, and 4 may imply eccentricity but never circularity. Variations in the fit to the secondary eclipse across different sectors were analyzed, and systems exhibiting changes beyond a certain threshold ($\Delta\phi=0.0002$) were flagged for potential apsidal motion. Additionally, since heartbeat phenomena occur exclusively in eccentric binaries, the detection of heartbeat signals in cases where only one eclipse was observed allowed us to identify the system as eccentric.

2.4. Spectroscopic observations and classification

To address the inconsistencies in spectral classifications found in the existing literature, we undertook the task of obtaining new spectra. Low-resolution spectra were obtained using the Jorge Sahade telescope at Complejo Astronómico El Leoncito (CASLEO) in San Juan, Argentina, utilizing the REOSC spectrograph in single mode alongside the new Sophia CCD. This equipment yielded spectra with a resolution of $R \sim 1000$, covering the wavelength range of 3760–5845 Å suitable for spectral classification in the MKK system. Spectral data processing was conducted in the standard way using [IRAF](#)¹ routines.

The resulting spectra are depicted in Fig. 1. They have been classified following the criteria described in [Walborn & Fitzpatrick \(1990\)](#); [Sota et al. \(2011, 2014\)](#). To summarize, we employed the ratio between He II $\lambda 4541$ and He I $\lambda 4387$, for late O-types, and Si III $\lambda 4552$ /Si IV $\lambda 4089$, for early B-types. Further details about spectral classification of OB stars can be found in the references provided.

The new spectral types are presented in the corresponding Tables 2, 3 and 4, column ST1, and are indicated with the label “tw”. No ST2 is given due to the low spectral resolution, which prevents the disentangling of both components in the system.

¹ NOIRLab IRAF is distributed by the Community Science and Data Center at NSF NOIRLab, which is managed by the Association of Uni-

3. Results

Among the 87 systems, this study reveals 20 new eclipsing binaries (Table 1), including 13 whose variable nature was previously unknown, five targets which were known as photometric variables or spectroscopic binaries, but not as DEB, and two of them were identified as nonthermal contact (because they present different light minima). Moreover, we introduce new LC classifications for 30 systems and report novel findings such as eccentricity in 13 systems, heartbeat features in 17, new types of variability in 11, and debut TESS LC presentations for the majority of the sample.

The study’s results are presented in three distinct tables: confirmed members of the catalog (Table 2), candidates pending spectral classification (Table 3), and unqualified candidates (Table 4). Confirmed members are systems that meet the essential conditions of displaying Algol-type LCs (detached) and having at least one component with a spectral classification within the O9–B1 V range. Candidates are also detached systems that show potential signs of meeting the spectral type criteria but lack definitive confirmation due to incomplete or inconclusive spectral classification. Unqualified systems are those whose LCs do not appear detached (EB or EW), have primary spectral classifications clearly out of range, or both. The secondary component’s classification might either be out of range or impossible to detect due to limitations in current spectroscopic data and analysis. While unqualified detached systems with indeterminate secondary classifications are currently unsuitable for the catalog, future higher-resolution or more sensitive spectra could reveal additional stellar features, prompting their reconsideration as candidates.

For each group, we detail findings from our photometric analysis, including delta magnitude (Δmag), period (P), time of minima (T_0), observed apsidal motion (Apsidal), additional system variability (MultiP), heartbeat phenomena (HB), and eccentricity (e). Additionally, we provide our spectral classifications for certain stars, either to fill gaps where classifications were absent or to verify existing classifications.

Regarding new spectral types, we confirmed HD 298448, CD-28 5257, HD 309036, V* IK Vel as entries to the YMDB (Table 2), and emphasize that certain eclipsing binary systems were excluded from the YMDB catalog because their spectral types fall outside the range studied here. An intriguing example is CM CMa (=Gaia DR3 2928505622380096256), which lacks a documented spectral type in the eight publications indexed in the Simbad database. Our April 2023 night spectrum reveals absorptions consistent with an F5 V type, characterized by similar H and K Calcium lines and the presence of the G-band. Another case is GN Nor (=Gaia DR3 5884730512723833984), which similarly lacks spectroscopic references in Simbad. Our CASLEO spectrum is classified as A0 V, primarily due to the dominance of Balmer lines. Similar cases are V* GN Nor and * f Vel, whose spectral classifications resulted out of the range for this catalog. These spectra are shown in Fig. 1.

In certain LCs, we observed additional variability beyond the typical eclipsing patterns. These variations, unless identified as heartbeat phenomena, are denoted with 1 in the tables. Therefore, we detected such oscillations in 37 systems, 11 of which are unprecedented. Most newly discovered pulsating systems have dedicated paragraphs, except HD 309036, HD 204827, all of them well known DEBs.

versities for Research in Astronomy (AURA) under a cooperative agreement with the U.S. National Science Foundation.

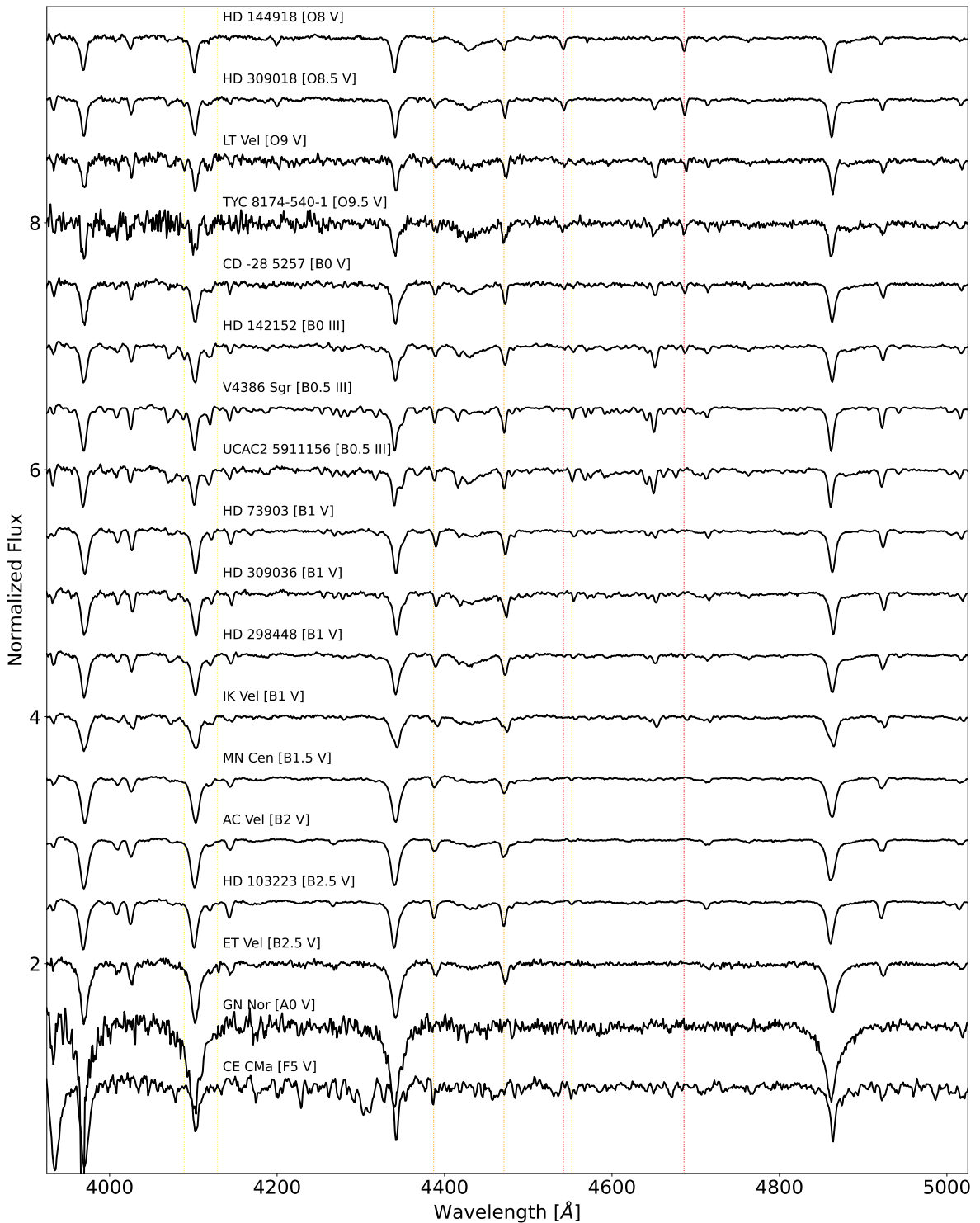


Fig. 1. CASLEO spectra classified in this work. Vertical lines indicate most important spectral lines used for classification, i.e., He II (in red), He I (orange), and Si II–III–IV (yellow).

Finally, the visual inspection of TESS LCs allowed us to detect apsidal motion. This phenomena is indicated in the tables (with 1) when the times of the secondary eclipses seem to vary among different sectors.

3.1. New detached eclipsing binaries discovered

We offer a detailed insight into select DEB featured within the YMDB.

BD+66 1674: Initially noted as a probable RV variable (Crampton & Fisher 1974), no additional references were found in the available literature. Although Maíz Apellániz et al. (2016) classified it as O9.7 IV, an analysis, incorporating high-resolution spectra from the Galactic O-Star Spectroscopic Survey (GOSSS; Maíz Apellániz et al. 2016) and the Library of Libraries of Massive-Star High-Resolution Spectra (LiLiMaRlin; Maíz Apellániz et al. 2019a), revealed it to be a B0 V + B0 V system (Maíz Apellániz, priv. comm.). Consequently, it has been

Table 1. Newly identified eclipsing binaries.

Simbad	RA	Dec	V
New variables discovered (DEB)			
BD+66 1674	00 02 10.2414	+67 25 45.186	9.6
BD+66 1675	00 02 10.2887	+67 24 32.228	9.08
HD 278236	05 26 55.2050	+40 32 53.088	10.86
RAFGL 5223	07 08 38.7906	-04 19 04.847	12.06
TYC 8174-540-1	09 20 18.7707	-49 50 25.869	11.63
HD 102475	11 47 18.1823	-62 26 10.246	9.09
HD 114026	13 08 44.0123	-60 20 18.400	9.36
CPD-63 3284	14 31 58.7177	-63 36 17.783	11.2
UCAC2 5911156	15 15 25.1420	-59 09 48.929	12.17
HD 142152	15 55 33.8521	-54 46 35.833	9.82
CD-54 6456	15 55 39.6014	-54 38 36.636	10.41
HD 144918	16 10 29.1581	-49 02 47.091	9.96
BD+55 2722	22 18 58.6254	+56 07 23.482	10.15
New eclipsing binaries discovered (DEB)			
HD 277878	05 18 22.7563	+41 56 06.000	10.27
* psi02 Ori	05 26 50.2293	+03 05 44.422	4.61
LS VI +00 25	06 48 50.4782	+00 22 37.694	10.86
CD-53 6352	16 00 26.8255	-53 54 39.860	10.4
HD 338961	19 50 24.4190	+27 27 55.913	10.86
New eclipsing binaries discovered (not DEB)			
LS V +38 12	05 20 00.6489	+38 54 43.505	10.4
HD 305850	11 01 52.2783	-60 00 46.795	8.8

Note: List of 20 eclipsing binaries identified in this study. This includes 13 binaries previously unrecognized as variables, five known either as photometric variables or spectroscopic binaries but not as DEBs, and two identified as nonthermal contact binaries.

included in the YMDB. Its LC displays additional variations beyond the 18-day eclipsing pattern, resembling those of highly eccentric detached double-eclipsing systems. Moreover, a notable bump between eclipses suggests the presence of a heartbeat-like feature (see Fig. 2). Considering the pixel size of TESS data, we conducted a search for other targets within a 40 arcsec radius and identified seven Gaia sources. These sources, at least four G-magnitudes fainter than BD+66 1674, complicate the determination of whether the short-period binary is one of these sources or an unresolved component of BD+66 1674.

BD +66 1675: Classified as O7.5 Vz (Maíz Apellániz et al. 2016), high-resolution spectra obtained within the context of LiLiMaRlin (Maíz Apellániz et al. 2019a) revealed BD +66 1675 to be a triple system comprised of O7.5Vz+O8V+B components. A preliminary analysis of 20 spectra indicated that the RV of the spectral lines belonging to the O7.5 Vz star do not vary within errors. However, the O8V + B pair exhibits RV motion in accordance with the photometric period. Moreover, preliminary orbital elements suggest an eccentric orbit, explaining why only one eclipse is observed. This eclipse occurs when the massive star passes in front of the system, making it a secondary eclipse. Also, we detect a heartbeat-like behavior immediately after the eclipses, but only in the Sector 58 (Fig. 3), and short-period variability identified as pulsations.

HD 278236: Classified as O9 V by Georgelin et al. (1973), no publications reporting variability or binarity were found. It is noteworthy that the relative position of the secondary eclipse appears to vary in different sectors, indicating apsidal motion (Fig. 4). Moreover, apsidal motion is making the secondary

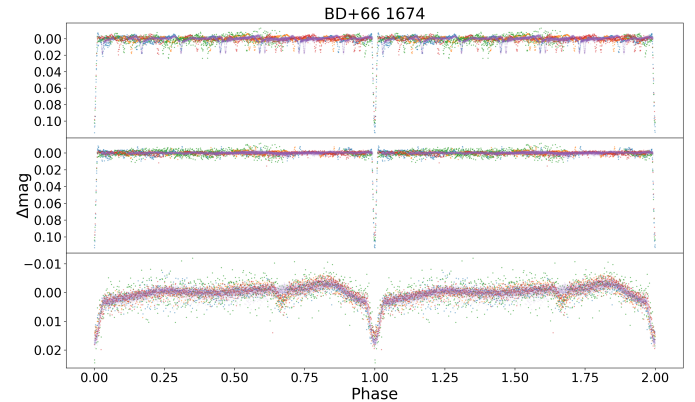


Fig. 2. Light curves of BD+66 1674. The top panel displays the composite LC, while the middle panel shows the LC corresponding to the B0 V+ B0 V system. In the bottom panel, the LC of the newly discovered eccentric short-period DEB system is depicted, with its sources unidentified as of yet. Each color represents a different sector of TESS.

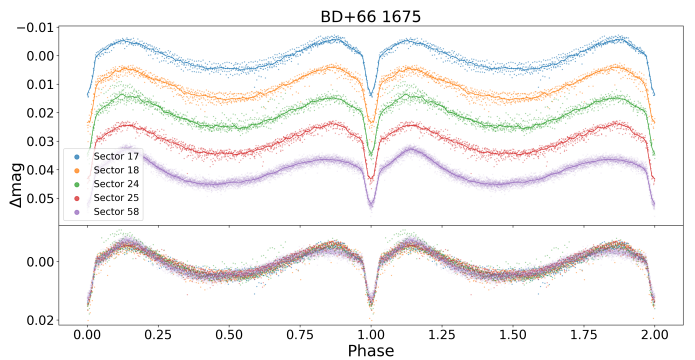


Fig. 3. Light curves of BD+66 1675. The top panel displays each reduced TESS sector separated by an artificial 0.01 Δ Mag for visibility. The composite LC is shown in the bottom panel. Sectors from 17 to 58 span 1150 days of observation. A heartbeat-like feature is present before the eclipse in the earliest sector (17), while the same feature is visible after the eclipse by the latest sector (58).

eclipse narrow overtime (from sector 17-59 ~1100 days and from 59-73 equivalent to ~1400 days, for a total time span of ~2500 days).

RAFGL 5223: Recognized as a Herbig Ae/Be star candidate, its entire bibliography is centered around this characteristic. However, no indications of variability, either spectroscopic or photometric, were identified. To scrutinize the indicated spectral classification in the Simbad database, we downloaded a X-Shooter spectrum (program ID 084.C-0952(A)) from the ESO portal. By evaluating the ratios between He II and He I pairs, we determined it to be of O9.2 type, with He II λ 4686/He I λ 4713 and Si IV λ 4089/He I λ 4026 ratios indicative of a V luminosity class. Consequently, it has been included in YMDB as an eccentric short-period binary. We note a potential heartbeat feature, manifested as a bump in the orbital phases where the periastron passage is expected. We also remark a probable apsidal motion, as separation between eclipses seems to vary among Sectors 7 and 33 (~700 d).

TYC 8174-540-1: Initially identified as an OB star by Muzzio & Orsatti (1977) and subsequently classified as O9.5 Vn by Bassino et al. (1982), TYC 8174-540-1's spectral type was verified through our own CASLEO spectrum (see Fig. 1). Despite an absence of reports regarding its binary nature, the

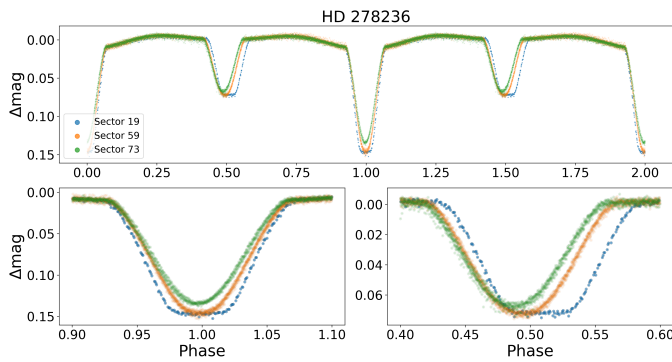


Fig. 4. Light curves of HD 278236. The top panel displays the composite LC of the system. Bottom left and right panels provide zoomed views of the primary and secondary eclipses, respectively. Observations from Sectors 19 to 73 span 1500 days. In the earliest sector (17) the eclipse exhibits a flat profile, indicative of a total eclipse. Over time the eclipse profile gradually smoothens, completely losing its flatness by the latest observed sector (73), indicative of a shift to a partial eclipse. Apsidal motion is also evident in this system, as demonstrated by the phase shift of the secondary eclipse.

TESS LC unmistakably depicts both eclipses, which, in fact, are transit and occultation events. This characteristic increases its significance as a benchmark for determining stellar parameters. Notably, the system exhibits eccentricity and appears to manifest a heartbeat phenomenon before entering the primary eclipse.

HD 102475: We found no evidence in the existing literature suggesting that it is a binary or variable star. It is only mentioned in general works on spectral types (Feast et al. 1961; Houk & Cowley 1975), where it is classified as B0.5 II and B1 III, respectively. Therefore, we include this target as a candidate until its spectral type is confirmed with modern spectroscopic analysis. It also exhibits short-period variability, interpreted as pulsations.

HD 114026: While we found no evidence suggesting variability, Garrison et al. (1983) identified it as a probable SB2 system. Despite its spectral classification exhibiting significant dispersion, ranging from OB to B2, with Garrison et al. (1983) designating it as a B0.5 V:n type, we prefer to be cautious and include HD 114026 as a candidate for the YMDB.

CPD –63 3284: This star lacks a reliable spectral classification, and unfortunately, we were unable to observe it during our run at CASLEO. Initially identified as an OB star by Lynga (1964), no additional classification information was found. Nevertheless, its LC unmistakably displays double eclipses, which indeed correspond to occultation and transit events. It also exhibits short-period variability, interpreted as pulsations. We include it as a candidate in the YMDB.

UCAC2 5911156: Initially recognized as an early-type star by Muzzio & Orsatti (1977) and subsequently classified as B0.5 V (Bassino et al. 1982), we acquired a new spectrum leading to a reclassification of its luminosity class to III. This adjustment is based on the almost similar intensities of the absorption lines He I λ 4387 and Si III λ 4552. The giant nature of UCAC2 5911156 naturally explains the pulsations noted in the LC shown in Fig. 5. The LC exhibits eclipses with a superimposed set of oscillations forming a beating pattern, akin to those initially discovered in HD187091 (Welsh et al. 2011; Thompson et al. 2012, and references therein). Notably, these damped oscillations do not align with the orbital period, as the maximum amplitudes do not occur at the same phase. To the best of our knowledge, this is the first identification of the system as a DEB and pulsating. However, a

detailed analysis of this intriguing system is beyond the scope of this work.

HD 142152: Initially classified as a B0 III massive star by Crampton (1971) and subsequently confirmed by Houk & Cowley (1975), HD 142152 lacked published spectra. To address this absence, we observed this target using CASLEO and confirmed its spectral classification (see Fig. 1). The identification as a probable binary arises from two discrepant radial velocities reported by Crampton (1972). The TESS LC distinctly illustrates a highly eccentric detached double-eclipsing behavior. Additionally, pulsation-like variations, occurring with 1/8 of the orbital periodicity, and a discernible heartbeat feature are detected. This renders the target exceptionally interesting, despite its exclusion from YMDB due to its luminosity class.

CD –54 6456: Prior to this study, there were no records indicating variability or binarity for this system. Classified as O9.5 V (Sota et al. 2014), our analysis involved six high-resolution spectra, which revealed no RV variations in the features of the O-type star. Consequently, this suggests that the eclipsing binary likely involves another stellar pair within the TESS pixel or is indistinguishable from CD –54 6456. For this reason, we have included it as a candidate in the YMDB.

HD 144918: This target exhibits one of the most widely scattered spectral type assignments in the literature, ranging from O5/7 (Houk 1978) to B0 (Cannon & Pickering 1921), with none originating from a modern study. Consequently, we decided to acquire a new spectrum. The CASLEO spectrum is classified as O8 V, with this classification based on the observation that He II λ 4542 is slightly fainter than He I λ 4471. Concerning its binary nature, it is reported as SB2 by Feast & Thackeray (1963), yet no period is provided, and no dedicated work was found in the literature.

BD +55 2722: This system is, indeed, a Trapezium-like configuration with components named A (O8 Vz), B (O9.5 V), and C (O7 V(n)z+B), according to the GOSSS (Mafz Apellániz et al. 2016). Given that the three sources are indistinguishable in TESS data, we attribute the DEB discovery to the C component, thereby designating BD +55 2722 C as a candidate in the YMDB. This classification stands until the spectral type of the secondary component is more precisely determined.

HD 277878: Despite extensive literature search, no evidence of photometric variability was found for this target. Originally identified as an OB or B0-type star, it was recently reclassified as O7 V((f))z based on LAMOST spectra (Li 2021), and indicated as SB1. Consequently, we have excluded it from consideration in the YMDB.

*** psi02 Ori:** It is a widely recognized spectroscopic binary (Plaskett 1908; Lu 1985), and also known to exhibit ellipsoidal variations (Avvakumova et al. 2013). In the TESS data, its double-eclipsing nature is clearly evident, alongside the ellipsoidal variations. However, due to its spectral type being identified as B1 III + B2 V (Lu 1985), we have excluded it from consideration in the YMDB.

LS VI +00 25: It was initially identified as an SB1 system by Munari & Tomasella (1999), although no photometric variations have been reported to our knowledge based on available literature. With a spectral type of O9.5 V (Li 2021), we have included it in the YMDB.

CD-53 6352: This star is recognized as double or multiple according to the Washington Double Star Catalog (WDS J16001-5355AB), but no photometric or RV variability has been identified. Analysis of TESS data has not conclusively determined whether star A or B is the DEB. While component A is classified as O7 III (Vijapurkar & Drilling 1993), the spectral

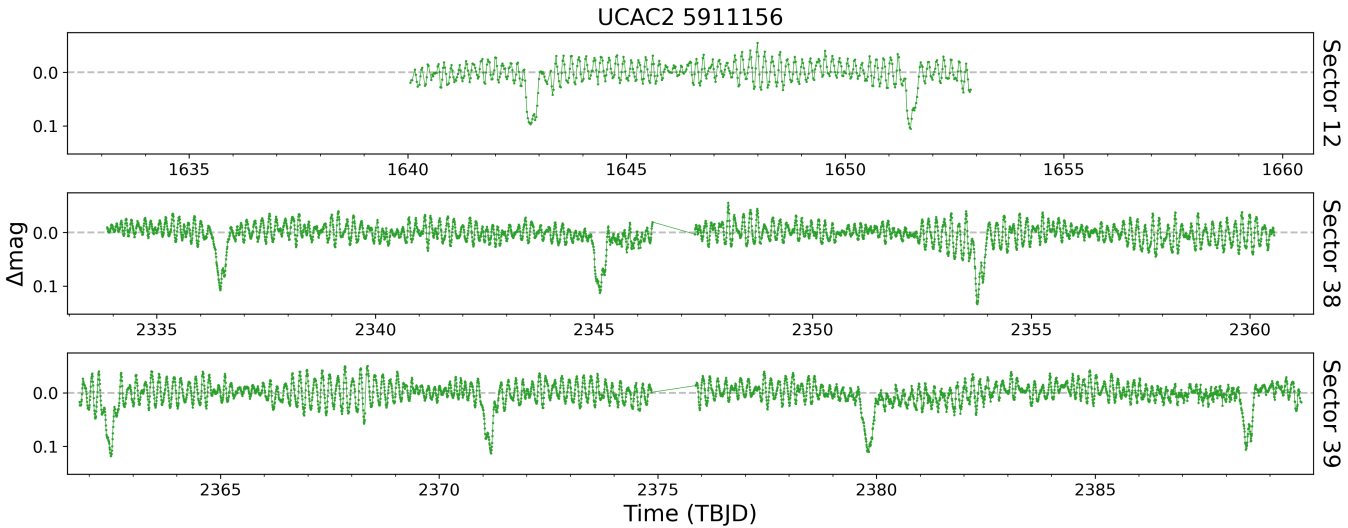


Fig. 5. Light curves of UCAC2 5911156. Panels top to bottom show the unfolded LCs of Sectors 12, 38, and 39 respectively. All panels maintain equal Y and X axis scales. This system exhibits pronounced Tidally Excited Oscillations (TEOs) in each sector, reflecting oscillations in the star or system caused by tidal interactions with a nearby stellar companion.

classification for component B is unavailable. As such, we have included it as a candidate in the YMDB. Additionally, its LC exhibits short-period variations compatible with pulsations.

HD 338961: No evidence of variability or binary nature was found for this star in the literature consulted. Despite some dispersion in its spectral classification, we consider the determination B0.5 III_n from (Turner 1980) to be reliable. Therefore, we have excluded it from inclusion in the YMDB.

3.2. Contact binary systems discovered

We provide details of two targets initially considered for inclusion in the YMDB. However, subsequent analysis of the TESS data revealed that they are contact binaries, leading to their rejection.

LS V +38 12: This star was identified as a binary system, based on spectroscopic observations, by Maíz Apellániz et al. (2016), who classified the pair as O7 V((f))+ B0 III-V.

HD 305850: It is listed as a pulsating star in Simbad, yet we found no references to its periodicity or LC. Moreover, its spectral type is actually uncertain, requiring an accurate determination.

3.3. DEBs showing heartbeat phenomena

In the YMDB, in addition to TYC 8174-540-1, RAFGL 5223, HD 142152, BD+66 1675 and the subsystem found within BD+66 1674 which are already detailed in 3.1, several other systems exhibit variations in their LCs consistent with the heartbeat phenomenon.

V* NY Cep: It is a well-known DEB (see e.g., Albrecht et al. 2011), characterized by a single eclipse resulting from its high eccentricity and periastron longitude. Notably, a bump is observed in its LC just before entering the eclipse, which we interpret as a probable heartbeat, although other proximity effects could not be discarded.

HD 99898: This star is a previously identified variable, classified as Algol type (Pojmanski 1998), and subsequently analyzed as a detached eclipsing binary (DEB) displaying apsi-

dal motion (Khaliullin et al. 2006). However, no heartbeat phenomenon was reported prior to this study.

CD-28 5257: It is a recognized eclipsing binary (see e.g., Pozo Nuñez et al. 2019), although the reported periodicity is incorrect. Our analysis reveals it to be an eccentric double-eclipsing system, with eclipses corresponding to both transits and occultations. Furthermore, a marginal bump is observed in the orbital phases where the expected periastron occurs, which we identify as a heartbeat effect, made possible by the precision of the TESS data. This star is marked for exhibiting apsidal motion in Table 2, as the orbital phases of the secondary transits appear to vary across available Sectors 7, 8, 34, and 61.

V* V725 Car: It is a DEB in a highly eccentric orbit, with an RV curve determined for its primary component (Kiminki & Smith 2018). The new LC presented here reveals a distinct heartbeat effect between the closer eclipses. An integrated analysis of both datasets, spectroscopic and photometric, will enable the determination of stellar parameters for both components.

V* Y Cyg: It is a well-established SB2 eclipsing binary (Sawyer 1887; Maíz Apellániz et al. 2019b). A marginal flux increase is observed at orbital phases corresponding to the periastron passage, which can be interpreted as a heartbeat effect, although it could also be attributed to ellipsoidal variations. This system exhibits apsidal motion, as evidenced by the variation in secondary eclipse times (and possibly their depths) between sectors 15 and 41 (~ 700 d).

CD -27 4726: It is a very well-known DEB. TESS data show an asymmetric light increasing just before and after the (unique visible) primary eclipse. Its shape reminiscences the one detected on the very massive binary system WR 21a (Barbá et al. 2022). Unluckily, the spectral type of this DEB is not completely reliable thus, we add CD -27 4726 to the candidates list.

HD 306096: It is also a very studied DEB, but we note a clear heartbeat feature on the orbital phases where the periastron passage is expected.

V* GN Nor: This is another well-known system; however, its heartbeat has not been reported to the best of our knowledge.

***f Vel:** It is a studied DEB system; however, as far as we are aware, its heartbeat phenomenon has not been documented.

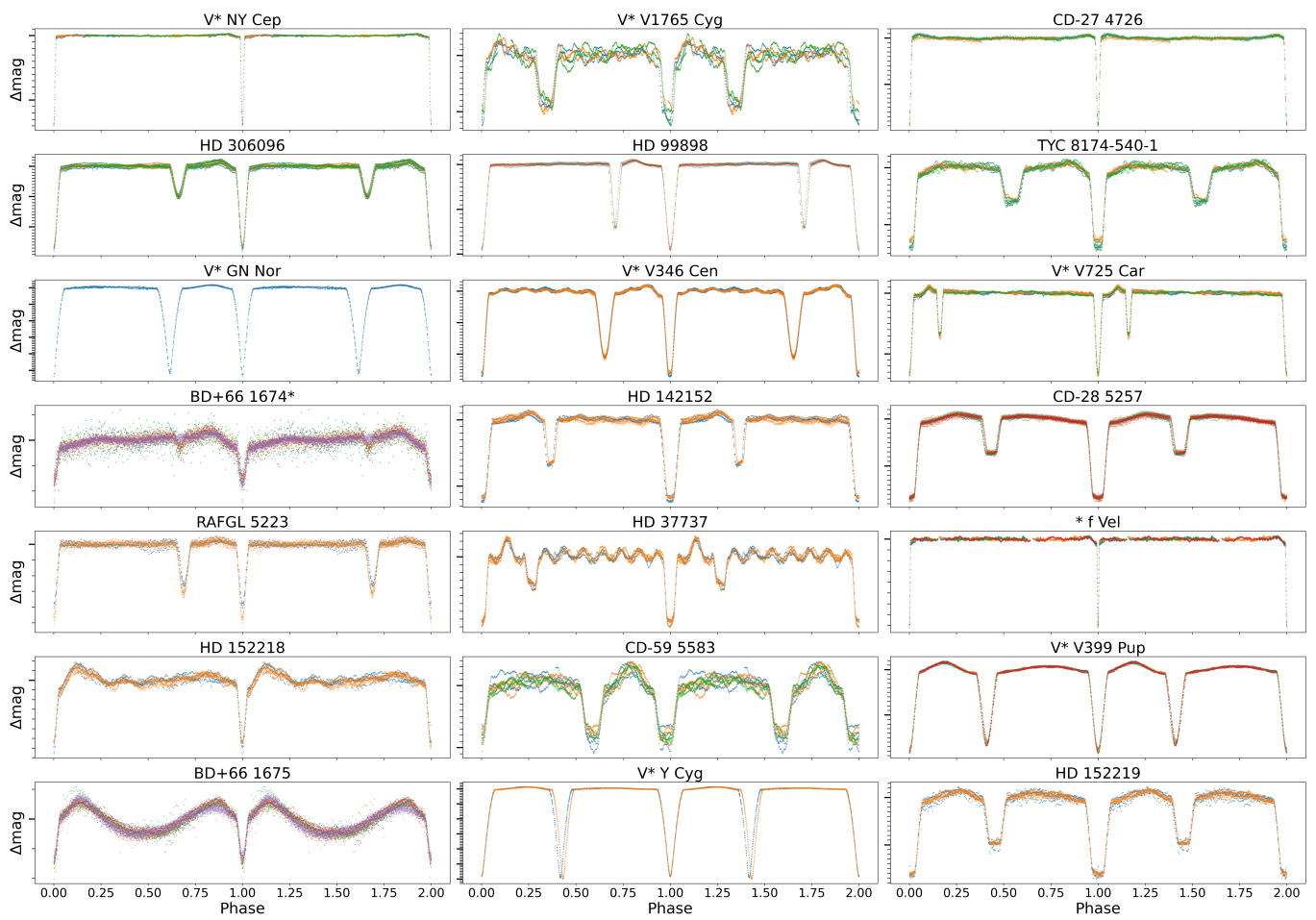


Fig. 6. Light curves of systems displaying heartbeat-like features. In each subpanel, bold, long ticks on the Y-axis denote increments of $0.1\Delta\text{mag}$, and thin, short ticks indicate increments of $0.01\Delta\text{mag}$.

3.4. DEBs with newly determined periods

We compared the periods obtained from our analysis of the TESS data with those previously published. Some of the periods we derived were found to be twice as long as the previously reported ones. This discrepancy is likely due to the improved depth and resolution of the eclipses identified in the TESS data, enabling a clearer distinction between primary and secondary eclipses. While we have already discussed these discrepancies for system CD-28 5257 in Section 3.3, we now address those for which we have not yet provided details.

V* KU Car: KU Car, reported as B8 in SIMBAD from [Avakumova et al. \(2013\)](#) and initially observed with a period of 5.92 days by [O'Connell \(1951\)](#), is reexamined in the author's Master's dissertation [Martín-Ravelo et al. \(2021\)](#). The dissertation utilized ASAS-3 data, which revealed a secondary eclipse previously unnoticed, effectively revising the reported period to 2.96 days. Detailed spectral analysis was performed using data from the Galactic O Star Spectroscopic Survey [Sota et al. \(GOSSS; 2011, 2014\)](#); [Maíz Apellániz et al. \(GOSSS; 2016\)](#), which led to a revised spectral classification of B0.5 V(n). While O'Connell previously suggested an eccentric orbit based on the LC's shape outside the eclipses, this hypothesis was biased by an incomplete understanding of the LC's true nature. Our observations do not indicate eccentricity from the LC; only a comprehensive RV study could resolve this ambiguity. Ongoing spec-

troscopic analysis aims to refine the temperature and absolute parameters of KU Car.

HD 99630: This star is known as DEB, but its periodicity is badly reported in the literature ([Pojmanski 1998](#); [Alfonso-Garzón et al. 2012](#)). Our analysis of the TESS LC reveals that its period is nearly double the previously reported value. Additionally, it shows double eclipses and high eccentricity. Our high-resolution spectra, obtained during the OWN Survey campaigns, indicate its spectral type is earlier than the B4-B5 determined by [Loden et al. \(1976\)](#). The ratio between He I $\lambda 4471$ and Mg II $\lambda 4481$ lines is greater than three, and C II $\lambda 4267$ is identified, thus a B3-type is more suitable. The weakness of the metal lines confirms its dwarf class, B3 V.

CD-59 3165: It is recognized as a highly eccentric DEB ([Kim et al. 2018](#)). In the TESS data, in addition to exhibiting double-eclipsing behavior, it also displays other eclipses with a periodicity of 3.18205 d (see Fig. 7). Given that this star is identified as a double in the WDS catalog (WDS J10348-6013AB), with both stars separated by only 2.3 arcseconds ([Mason et al. 2001](#)), we can not definitively confirm the origin of these additional eclipses. However, our analysis of two spectra obtained during opposite quadratures of the main DEB system as part of the OWN Survey program reveals distinct spectral features for each component. One component exhibits narrow lines, while the other shows broader lines. The ratio of Si III $\lambda 4552$ to Si IV $\lambda 4089$ is nearly unity in the narrow component, suggesting a spectral type of B0.5. Conversely, this ratio is smaller in the

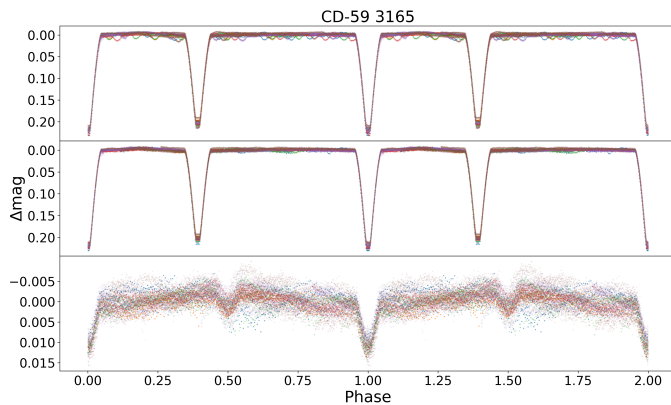


Fig. 7. Light curves of CD-59 3165. The top panel displays the composite LC. The middle panel illustrates the LC for the system with a period of 7.59 days, while the bottom panel shows the system with a period of 3.18 days. Each color represents a different sector of TESS

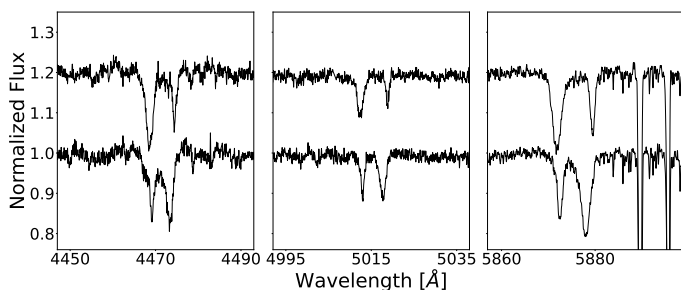


Fig. 8. Three wavelength regions, around selected He I absorption lines of two spectra of CD -59 3165 obtained during quadratures.

broader component, and considering the absence of He II $\lambda 4542$, yield a spectral type of B0-0.2. In terms of luminosity class, the narrow component appears to belong to classes III-I, as He II $\lambda 4686$ is markedly fainter than He I $\lambda 4713$. Conversely, both lines are comparable in the broad component, indicative of a class V classification. In Fig. 8 we show some spectral regions to illustrate these classifications. In the future, we plan to conduct a more targeted spectral analysis to identify the spectral signatures of both components of the other DEB system. This analysis will also aim to elucidate the source of the additional eclipses observed.

3.5. Other intriguing systems

We identified a diverse set of interesting systems, each presenting unique photometric characteristics that merit special mention. Firstly, several systems in our sample displayed Tidally Excited Oscillations (TEOs), which are oscillations within a star or system driven by tidal forces due to a close stellar companion. Notable examples include UCAC2 5911156 (detailed in 3.1, Fig. 5) along with V* V4386 Sgr, 2MASS J16542949-4139149, * 23 Ori, and V* V1216 Sco.

Additionally, we have successfully disentangled LCs of systems where the combined photometric data initially obscured individual components. Systems such as CD-59 3165 (detailed in 3.4, Fig. 7), BD+66 1674 (3.1, Fig. 2) and eta Ori (detailed below, Fig. 10).

We also observed systems whose eclipse characteristics vary significantly over time, adding another layer of complexity to their study. For instance, HD 278236 initially showed flat

eclipses typical of total eclipses but over a span of 1500 days, the eclipse profile gradually transitioned to partial, with a smoothing and narrowing that indicates dynamic changes in the system. Additionally, the shifting of the secondary eclipse suggests apsidal motion, highlighting the system's evolving orbital dynamics. (Fig. 4). HD 93683 exhibited a decrease in eclipse depth over 1500 days, suggesting changes in the system's configuration or surrounding material (Fig. 9). And BD+66 1675 (detailed in 3.1, Fig. 3) presented a heartbeat-like feature post-primary eclipse, which shifted to prior the eclipse over 1150 days of observation.

HD 93683: It is recognized as a SB2 system with a Be-type third component (Alexander et al. 2016; Bodensteiner et al. 2020). Our analysis of the TESS data unveiled intriguing behavior in this system, characterized by an attenuation of its eclipses (Fig. 9). This phenomenon could arise from variations in the brightness of the variable Be-star (either the star itself or its surrounding disk), which may dilute the eclipses. Alternatively, it could result from a rare effect known as Zeipel-Lidov-Kozai cycles, induced by the third component in a noncoplanar orbit, leading to changes in the orbital plane relative to our line of sight. As far as we know, this is the very first case reported in massive systems (see e.g., Borkovits et al. 2022, and references therein). This multiple system also exhibits several short-period variations, interpreted as pulsations. Shi et al. (2022) reported one such variation with a period of 2.4 days. Further analysis is needed to determine additional periodicities in the TESS data.

*** eta Ori:** *Eta Ori is an ideal candidate for our catalog as it meets the criteria of a detached binary with spectral types B0.7 V and B1.5: V. Southworth & Bowman (2022) analyzed TESS data and fitted the LC to obtain absolute parameters for the system, opting not to use data from sector 32 due to its low variability amplitude. In our study, we present LCs using both sectors (Fig. 10). We confirm the periodic variations reported in the literature: the primary eclipse cycle at approximately 7.989 days, indicative of the detached eclipsing binary (EB) system, and a shorter cycle of about 0.432 days, associated with pulsational variability. Lee et al. (1993) initially suggested that the shorter period might indicate a contact binary with a period of 0.864 days. Southworth proposed the configuration as a detached EB with a period of 7.988 days, where one component exhibits g-mode pulsations, alongside a noneclipsing binary with a period of 0.8641 days, showing strong ellipsoidal variations.

4. The Young Massive Detached Binary catalog

This work presents the comprehensive YMDB catalog, derived from the analysis of TESS LCs and spectroscopic data, with additional support from an extensive review of existing literature.

Eclipsing binaries offer a unique opportunity to determine stellar parameters with high precision, especially when combining LC information with RV data. Detached binaries are particularly valuable due to the minimal interaction between their stellar components, allowing for accurate determinations of stellar parameters.

Although systems within the O8–B3 spectral-type range are common, few have had their absolute parameters precisely measured. The YMDB catalog addresses this knowledge gap by providing a curated database of young massive detached binaries, facilitating high-precision stellar parameter determinations.

Through the analysis of TESS LCs for 87 systems with suspected spectral types in the range O9–B1, this study identified 20 new eclipsing binaries, including 13 previously unknown variable systems and 2 nonthermal contact binaries. Additionally, new LC classifications were reported for 30 systems, and novel

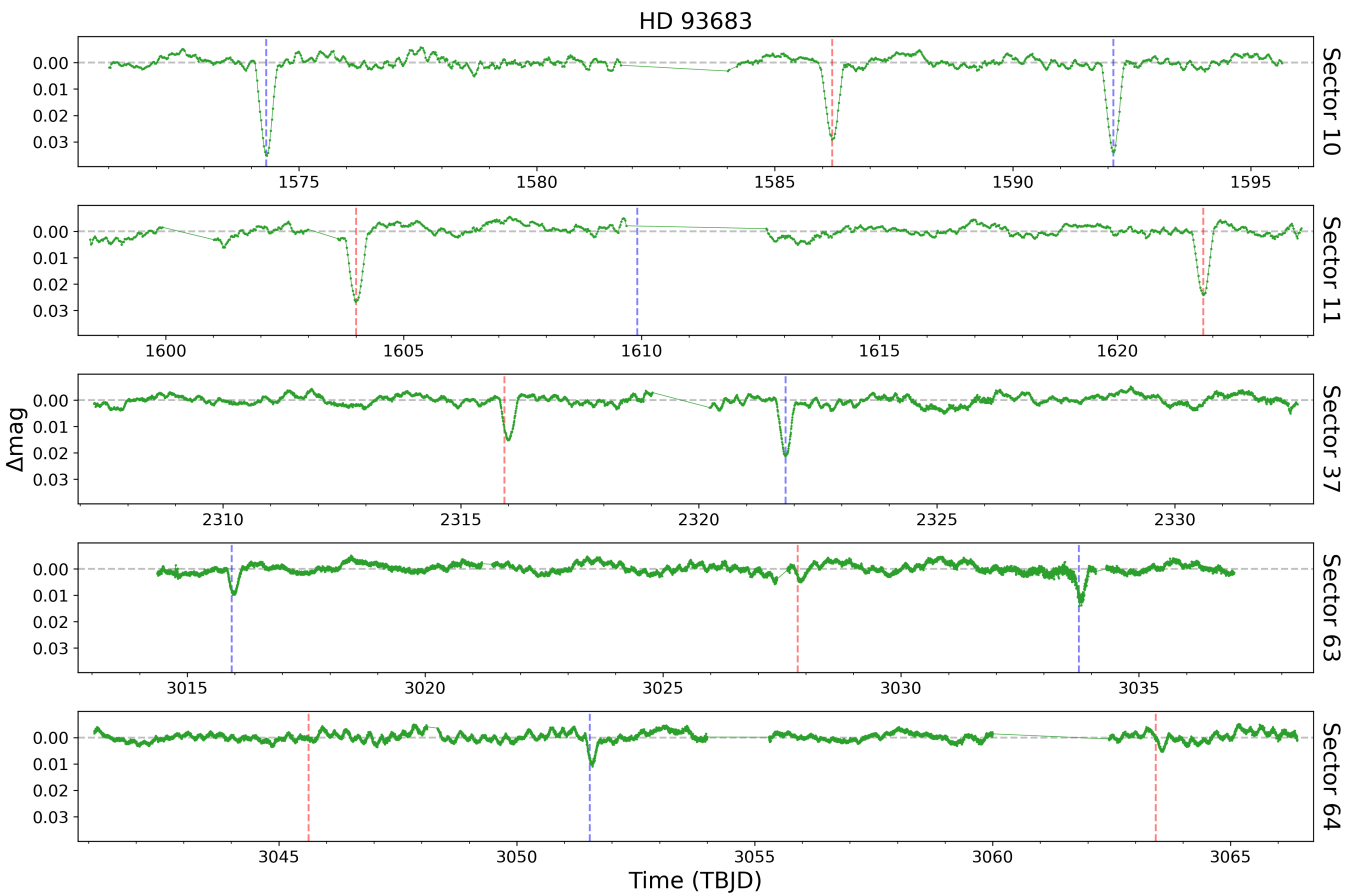


Fig. 9. Light curves of HD 93683. Each panel represents a different TESS sector, arranged chronologically from top to bottom. Predicted timings for the primary and secondary eclipses are marked with blue and red dashed vertical lines, respectively. All panels maintain equal Y and X axis scales. Over 1500 days, both primary and secondary eclipses consistently decrease in depth from approximately $0.3\Delta\text{mag}$ to around $0.1\Delta\text{mag}$, with the secondary eclipses being shallower overall. By the latest sector (64), the depth of the eclipses approaches the level of the system's intrinsic variability, rendering the first secondary eclipse undetectable. Apsidal motion is evident as early as Sector 37 when compared to Sector 10, although data from later sectors are not reliable for further apsidal motion analysis.

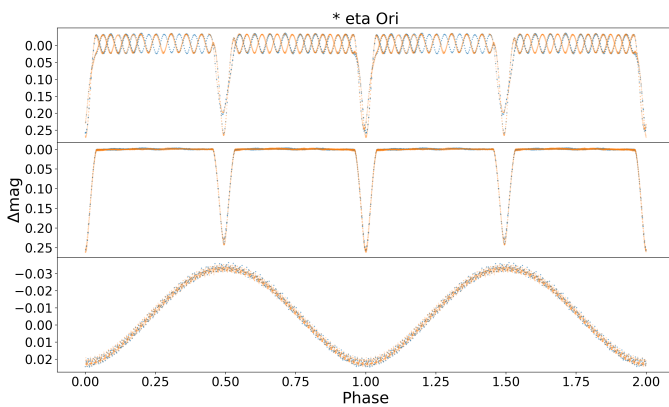


Fig. 10. Light curves of * eta Ori. The top panel displays the composite LC. The middle panel illustrates the LC for the eclipsing system with a period of 7.989 days disentangled from the shorter period pulsations, while the bottom panel shows such pulsations folded with period of 0.432 days. Each color represents a different sector of TESS

features such as eccentricity and heartbeat phenomena were discovered in many targets.

The YMDB catalog offers a reliable resource of high-quality LCs, serving as a valuable asset for the astronomical commu-

nity. The primary results of this study are documented in Table 2, which lists the 30 confirmed members of the YMDB. These systems feature detached LCs and have at least one component with a spectral classification within the specified range. For the 25 systems that show potential yet require further spectroscopic verification, details can be found in Table 3. The 32 systems that do not qualify for the catalog due to nondetached configurations or incompatible spectral types are included in Table 4

It is our desire to further calibrate this method and publish a semiautomatic pipeline for public use.

Acknowledgements. RG acknowledges support from grant PICT 2019-0344. JIA acknowledges the financial support of DIDULS/ULS, through the project PR2324063. This research made use of Lightkurve, a Python package for Kepler and TESS data analysis (Lightkurve Collaboration, 2018). This work made use of Astropy:² a community-developed core Python package and an ecosystem of tools and resources for astronomy (Astropy Collaboration et al. 2022).

References

Albrecht, S., Winn, J. N., Carter, J. A., Snellen, I. A. G., & de Mooij, E. J. W. 2011, *ApJ*, 726, 68
 Alexander, M. J., Hanes, R. J., Povich, M. S., & McSwain, M. V. 2016, *AJ*, 152, 190

² <http://www.astropy.org>

Table 2. Confirmed systems in the YMDB catalog.

SIMBAD	ΔMag	P	T0	Apsidal	Multi_P	HB	e	ET	ST1	ST2
V* NY Cep	0.140	15.2759	1768.17910		0	1	1	EA1	B0.5V	B2V
HD 99898	0.206	5.04950	2324.03500	1	0	1	1	EA2	B0V	
V* V404 Vel	0.103	11.4243	1518.04660		0	0	1	EA2	B0V	
HD 298448	0.142	2.31530	1545.16410		0	0	1	EA2	B1 V ^{tw}	
V* KU Car	0.574	2.96059	1571.58360		0	0	0	EA2	B0.5 V(n)	
BD+66 1674	0.123/0.017	18.8292 / 2.6395	1783.81040 / 2887.35633		0 / 1	0 / 1	- / 1	EA1 / EA2	B0 V ^{tw}	B0 V ^{tw}
V* V1208 Sco	0.124	5.21970	2387.49300		0	0	0	EA2	B0.5 V	*
V* AH Cep	0.308	1.77478	1792.24979		0	0	0	EA2	B0.2 V	B2 V
V* DW Car	0.647	1.32774	1597.83274		0	0	0	EA2	B1 V	B1 V
eta Ori	0.308 / 0.061	7.9886 / 0.4321	1472.43778 / 1469.94135		1	0	1 / 0	EA2 / EW	B0.7 V	B1.5: V
del Pic	0.243	1.67254	2389.11655		1:	0	0	EA2	B0.5 V	B0.5-3
V* VV Ori	0.310	1.48538	2199.25573		1	0	0	EA2	B1 V	B4.5 V
HD 338936	0.417	7.670	2771.85150		1	0	1	EA2	B0.5 V db	
TYC 8174-540-1	0.162	5.04690	1546.33040		1	1	1	EA2	O9.5 V ^{tw}	
LS VI +00 25	0.057	11.0287	2221.42860		0	0	1	EA2	O9.5 V	
HD 278236	0.157	1.99270	1816.47898	1	0	0	1	EA2	O9 V	
CD-28 5257	0.196	3.10894 / 3.38:	2253.54773 / 1498.46100	1	1	1	1	EA2	B0 V ^{tw}	
HD 93683	0.041:	17.7978	1574.31401	1	1	0	1	EA2	O9 V	B0 V
HD 152218	0.089	5.60410	1649.95040		1	1	1	EA1	O9 IV	O9.7 V
V* V346 Cen	0.293	6.322	1570.60040		1	1	1	EA2	B0.5 IV	B2 V
CD-35 4470	0.372	9.3535	1539.49440		0	0	1	EA2	B0 IV	
HD 309036	0.232	2.31525 / 0.12398	2356.19344		1	0	0	EA2	B1 V ^{tw}	
V* IK Vel	0.874	1.99232	1518.81743		0	0	0	EA2	B1 V ^{tw}	
RAFGL 5223	0.053	3.55907	1494.99690	1:	0	1	1	EA2	O9 V ^{tw}	*
Schulte 27	0.629	1.46920	1683.74890		0	0	0	EA2	O9.7V(n)	O9.7V(n)
V* HH Car	0.281	3.23146	1599.54000		0	0	0	EA2	O9 V	B0 III-IV
V* V1295 Sco	0.218	2.15764	1627.79500		0	0	0	EA2	O9.7 V	*
V* V725 Car	0.152	9.4106	1570.04690		0	1	1	EA2	O9.7 IV	*
V* Y Cyg	0.614	2.99625	1711.75278	1	0	1	1	EA2	O9.5 IV	O9.5 IV
HD 204827	0.011	3.0480	1743.64949		1	0	0	EA2	O9.5IV	*

Note: Summarized version of the YMDB catalog for confirmed systems. The table includes Delta magnitude (Δmag), orbital Period (P), and Time of minimum light (T0) from extracted TESS LCs. Identified features such as Apsidal motion, additional variability (Multi_P), Heartbeat-like features (HB), and Eccentricity (e) are presented with “1” indicating detection and “0” indicating non-detection. The Eclipsing Type (ET) is indicated as EA (Algol), EB (Beta Lyrae), or EW (W Ursa Majoris type), followed by “2” if both primary and secondary eclipses are visible, or “1” if only one is visible. A “/” between types indicates multiple discernible variations from the TESS LC. Spectral types for primary and secondary components are provided, with classifications performed in this work marked with “^{tw}”. An asterisk “*” instead of a spectral type indicates significant dispersion among various reliable sources, without a clear consensus. Uncertainties across the table are indicated by “:”. Full details, error margins, and sources for spectral types not classified in this work are available in the CDS extended version.

Table 3. Unconfirmed systems (candidates) for the YMDB catalog.

SIMBAD	ΔMag	P	T0	Apsidal	Multi_P	HB	e	ET	ST1	ST2
2MASS J16542949-4139149	0.182	6.34877	1633.56460		1	0	0	EA2	*	
HD 114026	0.230	2.1620	2334.09192		0	0	0	EA2	B0.5 V:n	
CPD-58 2608A	0.052	2.23284	2331.83340	1:	1:	0	1	EA2	*	*
V* V1153 Cen	0.557	5.979	2335.72810		0	0	1	EA2	*	
V* V1765 Cyg	0.164	13.3724	2794.57244		1	1	1	EA2	B0.5Ib	B2:V:
CD-27 4726	0.120	7.9587	1498.98070		0	1:	1:	EA1	*	
HD 306096	0.304	5.38300	1574.47920		0	1	1	EA2	B0	
V* GN Nor	0.559	5.703	1626.08130		0	1	1	EA2	A0 V: ^{tw}	
V* V1103 Cas	0.566	6.178	1790.53260		0	0	1	EA2	B0	
CD-59 3165	0.240 / 0.015:	7.59370 / 3.18206	1573.18250 / 1616.16205		0 / 0	0 / 0	1 / 0	EA2 / EA2	*	
V* CE CMa	0.638	27.0729	2247.82650		0	0	1	EA2	*	
HD 52504	0.381	1.42147	2225.87947		0	0	0	EA2	B1: V:	-
V* V646 Cas	0.471	6.16200	2006.30329		0	0	0	EA2	B0 IV:nn	
CPD-42 2880	0.095	1.8988	1566.58619		0	0	0	EA2	O9.5-B2	
CPD-63 3284	0.167	2.872	2359.61038		1	0	0	EA2	OB	
HD 111825	0.227	2.00669	1596.80501		0	0	0	EA2	*	
CD-54 6456	0.097	16.9742	1634.97340		0	0	1	EA2	*	*
HD 102475	0.012	9.0411	2324.78323		1	0	-	EA1	*	*
HD 152219	0.192	4.24024	2364.88748		1	1	1	EA2	O9.5 III	B1-2 V-III
V* EV Vul	0.863	2.82212	2421.09141		1	0	0	EA2	*	*
V* V499 Sco	0.501	2.33329	2389.56663		0	0	0	EA2	*	*
f Vel	0.086	26.3060	2302.27932		0	1	1	EA1	O9.7 II ^{tw}	B0 V: ^{tw}
V* XZ Cep	0.863	5.0973	1982.06212		0	0	0	EA2	B1.5 II-III	B1.1 III-V
BD+66 1675	0.029	2.71564	1768.18230		1	1:	1:	EA1	O8 V	B
BD+55 2722	0.036	2.00453	2881.12965		1	0	0	EA2	O7 Vz(n)	B

Note: Summarized version of the YMDB catalog for unconfirmed systems (candidates). Presented in the same format as Table 2.

Table 4. Unqualified systems for the YMDB catalog.

SIMBAD	ΔMag	P	T0	Apsidal	Multi_P	HB	e	ET	ST1	ST2
V* AC Vel	0.442	4.562	2284.25847		0	0	0	EA2	B2 V ^{tw}	
HD 52533	0.447	21.9648	1501.65900		0	0	1	EA2	O8.5IVn	
23 Ori	0.039	4.55520	1470.80658		1	0	0	EA2	B2 IV/V	*
HD 309018	0.052:	0.89216	2358.72842		0	0	1	EA2	O8.5 V ^{tw}	
HD 144918	0.059	1.27913	1625.75646		0	0	0	EA2	O8 V ^{tw}	*
V* V340 Mus	0.076	3.42725	1597.38243		1	0	0	EA2	O9 IV	*
V* FM CMA	0.239	2.78940	1509.69900	1	0	0	0	EA2	B2 IV ^{tw}	B3 V: ^{tw}
V* ET Vel	0.657	3.08090	1519.76470		0	0	1	EA2	B2.5 V ^{tw}	
HD 305850	0.086	2.3810	1620.65763		0	0	0	EB2	*	
V* V1082 Sco	0.402	23.4465	1637.81050		1	0	1	EA2	B0.5Ib	O9.5 III
HD 99630	0.214	21.1220	1602.84699		0	0	1	EA2	B4-B5	
UCAC2 5911156	0.189	8.6715	2379.81580		1	0	-	EA1	B0.5 III ^{tw}	
CD-53 6352	0.034	2.48610	1630.08061		1	0	0	EA2	O7III (for component A)	
CPD-64 1885	0.292	5.13930	1600.42950		0	0	0	EA2	B4-B6	
HD 277878	0.019	0.82253	2934.44773		1:	0	0	EA2	O7 V((f))z	
CD-59 5583	0.149	8.7060	2387.67312		1	1	1	EA2	B0II	
HD 338961	0.186	1.70970	2793.63189		0	0	0	EA2	B0.5 Illnn	
V* V1216 Sco	0.499	3.92060	2389.62316		1	0	0	EA2	B0.5III	
V* V421 Pup	0.137	5.41650	1500.20265		1	0	0	EA2	B1II	
HD 103223	0.332	2.54155	2358.08085		0	0	0	EA2	B2.5 V ^{tw}	
V* V1290 Sco	0.116	4.49260	1627.90670		1	0	0	EA2	O9.7 III	*
V* V4386 Sgr	0.231	10.802	1664.15850		1	0	0	EA2	B0.5 III ^{tw}	*
HD 142152	0.139	5.68640	1626.34840	1	1	1	1	EA2	B0 III ^{tw}	*
HD 37737	0.119	7.85199 / 1/10P / 3P	1821.42367		1	1	1	EA2	O9.5II-III(n)	*
V* V399 Pup	0.204	3.91019	2276.30939	1	0	1	1	EA2	B2 II	*
V* CC Cas	0.145	3.3670	1818.57209		1	0	0	EA2	O8.5III(n)((f))	*
V* MN Cen	0.587	3.48915	2359.82698		0	0	0	EA2	B1.5 V ^{tw}	*
V* V877 Cen	0.636	5.35857	2355.76939		0	0	0	EA2	B1III(n)	*
psi02 Ori	0.037	2.52596	2199.90592		1	0	1	EA2	B1 III	B2 V
u Her	0.663	2.05102	2767.92462		0	0	0	EA2	B2 IV	B8 III
LS V +38 12	0.053	1.42287	1837.24509		0	0	0	EB2	O7 V ((f))	B0III- V
HD 185780	0.024	3.51160	2822.28161		1	0	0	EA2	B0 III	*

Note: Summarized version of the YMDB catalog for unqualified systems. Presented in the same format as Table 2.

Alfonso-Garzón, J., Domingo, A., Mas-Hesse, J. M., & Giménez, A. 2012, A&A, 548, A79

Astropy Collaboration, Price-Whelan, A. M., Lim, P. L., et al. 2022, ApJ, 935, 167

Avvakumova, E. A., Malkov, O. Y., & Kniazev, A. Y. 2013, Astronomische Nachrichten, 334, 860

Barbá, R. H., Gamen, R., Arias, J. I., & Morrell, N. I. 2017, in The Lives and Death-Throes of Massive Stars, ed. J. J. Eldridge, J. C. Bray, L. A. S. McClelland, & L. Xiao, Vol. 329, 89–96

Barbá, R. H., Gamen, R. C., Martín-Ravelo, P., Arias, J. I., & Morrell, N. I. 2022, MNRAS, 516, 1149

Bassino, L. P., Dessaunet, V. H., Muzzio, J. C., & Waldhausen, S. 1982, MNRAS, 201, 885

Bodensteiner, J., Shenar, T., & Sana, H. 2020, A&A, 641, A42

Borkovits, T., Rappaport, S. A., Toonen, S., et al. 2022, MNRAS, 515, 3773

Cannon, A. J. & Pickering, E. C. 1921, Annals of Harvard College Observatory, 96, 1

Chini, R., Hoffmeister, V. H., Nasser, A., Stahl, O., & Zinnecker, H. 2012, MNRAS, 424, 1925

Crampton, D. 1971, AJ, 76, 260

Crampton, D. 1972, MNRAS, 158, 85

Crampton, D. & Fisher, W. A. 1974, Publications of the Dominion Astrophysical Observatory Victoria, 14, 283

de Mink, S. E., Langer, N., & Izzard, R. G. 2011, Bulletin de la Societe Royale des Sciences de Liege, 80, 543

Ekström, S. 2021, Frontiers in Astronomy and Space Sciences, 8, 53

Feast, M. W., Stoy, R. H., Thackeray, A. D., & Wesselink, A. J. 1961, MNRAS, 122, 239

Feast, M. W. & Thackeray, A. D. 1963, MmRAS, 68, 173

Gamen, R., Barbá, R., Morrell, N., et al. 2007, Spectroscopic monitoring of Southern Galactic O and WN stars: State of the Art in 2007

Gamen, R., Barbá, R. H., Morrell, N. I., Arias, J., & Maíz Apellániz, J. 2008, in Revista Mexicana de Astronomía y Astrofísica Conference Series, Vol. 33, Revista Mexicana de Astronomía y Astrofísica Conference Series, 54–54

Garrison, R. F., Schild, R. E., & Hiltner, W. A. 1983, ApJS, 52, 1

Georgelin, Y. M., Georgelin, Y. P., & Roux, S. 1973, A&A, 25, 337

Herrero, A., Kudritzki, R. P., Vilchez, J. M., et al. 1992, A&A, 261, 209

Houk, N. 1978, Michigan catalogue of two-dimensional spectral types for the HD stars

Houk, N. & Cowley, A. P. 1975, University of Michigan Catalogue of two-dimensional spectral types for the HD stars. Volume I. Declinations -90_ to -53_f0.

Khaliullin, K. F., Antipin, S. V., & Khaliullina, A. I. 2006, Astronomy Letters, 32, 772

Kim, C. H., Kreiner, J. M., Zakerzowski, B., et al. 2018, ApJS, 235, 41

Kiminki, M. M. & Smith, N. 2018, MNRAS, 477, 2068

Lee, W. B., Sung, E. C., Koch, R. H., et al. 1993, in Astronomical Society of the Pacific Conference Series, Vol. 38, New Frontiers in Binary Star Research, ed. K.-C. Leung & I.-S. Nha, 239

Li, G.-W. 2021, ApJS, 253, 54

Lightkurve Collaboration, Cardoso, J. V. d. M., Hedges, C., et al. 2018, Lightkurve: Kepler and TESS time series analysis in Python, Astrophysics Source Code Library

Loden, L. O., Loden, K., Nordstrom, B., & Sundman, A. 1976, A&AS, 23, 283

Lu, W. 1985, PASP, 97, 428

Luger, R., Agol, E., Kruse, E., et al. 2016, AJ, 152, 100

Luger, R., Kruse, E., Foreman-Mackey, D., Agol, E., & Saunders, N. 2018, AJ, 156, 99

Lynga, G. 1964, Meddelanden fran Lunds Astronomiska Observatorium Serie II, 141, 1

Maíz Apellániz, J., Sota, A., Arias, J. I., et al. 2016, ApJS, 224, 4

Maíz Apellániz, J., Trigueros Páez, E., Jiménez Martínez, I., et al. 2019a, in Highlights on Spanish Astrophysics X, ed. B. Montesinos, A. Asensio Ramos, F. Buitrago, R. Schödel, E. Villaver, S. Pérez-Hoyos, & I. Ordóñez-Etxeberria, 420–420

Maíz Apellániz, J., Trigueros Páez, E., Negueruela, I., et al. 2019b, A&A, 626, A20

Martín-Ravelo, P., Barbá, R., Rodolfo, H., Morrell, N., Arias, J., & Gamen, R. 2021, in MOBSTER-1 virtual conference: Stellar Variability as a Probe of Magnetic Fields in Massive Stars, 36

Martins, F. & Palacios, A. 2013, A&A, 560, A16

Mason, B. D., Wycoff, G. L., Hartkopf, W. I., Douglass, G. G., & Worley, C. E. 2001, AJ, 122, 3466

Munari, U. & Tomasella, L. 1999, A&A, 343, 806

Muzzio, J. C. & Orsatti, A. M. 1977, AJ, 82, 474

O'Connell, D. J. K. 1951, Publications of the Riverview College Observatory, 2, 85

Plaskett, J. S. 1908, ApJ, 28, 266

Pojmanski, G. 1998, Acta Astron., 48, 35

Pourbaix, D., Tokovinin, A. A., Batten, A. H., et al. 2004, A&A, 424, 727

Pozo Nuñez, F., Chini, R., Barr Domínguez, A., et al. 2019, MNRAS, 490, 5147

Sana, H., de Mink, S. E., de Koter, A., et al. 2012, Science, 337, 444

Sawyer, E. F. 1887, AJ, 7, 116

Shi, X.-d., Qian, S.-b., & Li, L.-J. 2022, ApJS, 259, 50

Simón-Díaz, S., Castro, N., García, M., Herrero, A., & Markova, N. 2011, Bulletin de la Societe Royale des Sciences de Liege, 80, 514

Sota, A., Maíz Apellániz, J., Morrell, N. I., et al. 2014, ApJS, 211, 10

Sota, A., Maíz Apellániz, J., Walborn, N. R., et al. 2011, ApJS, 193, 24

Southworth, J. & Bowman, D. M. 2022, MNRAS, 513, 3191

Thompson, S. E., Everett, M., Mullally, F., et al. 2012, ApJ, 753, 86

Trigueros Páez, E., Barbá, R. H., Negueruela, I., et al. 2021, A&A, 655, A4

Turner, D. G. 1980, ApJ, 235, 146

Vijapurkar, J. & Drilling, J. S. 1993, ApJS, 89, 293

Walborn, N. R. & Fitzpatrick, E. L. 1990, PASP, 102, 379

Weidner, C. & Vink, J. S. 2010, A&A, 524, A98

Welsh, W. F., Orosz, J. A., Aerts, C., et al. 2011, ApJS, 197, 4

Appendix A: Folded light curves for all 87 systems analyzed in this study

The appendix presents the LCs for all systems analyzed in this study. Figure A.1 shows the LCs for the confirmed systems, Figure A.2 displays the LCs for the candidate systems, and Figure A.3 includes the LCs for the unqualified systems.

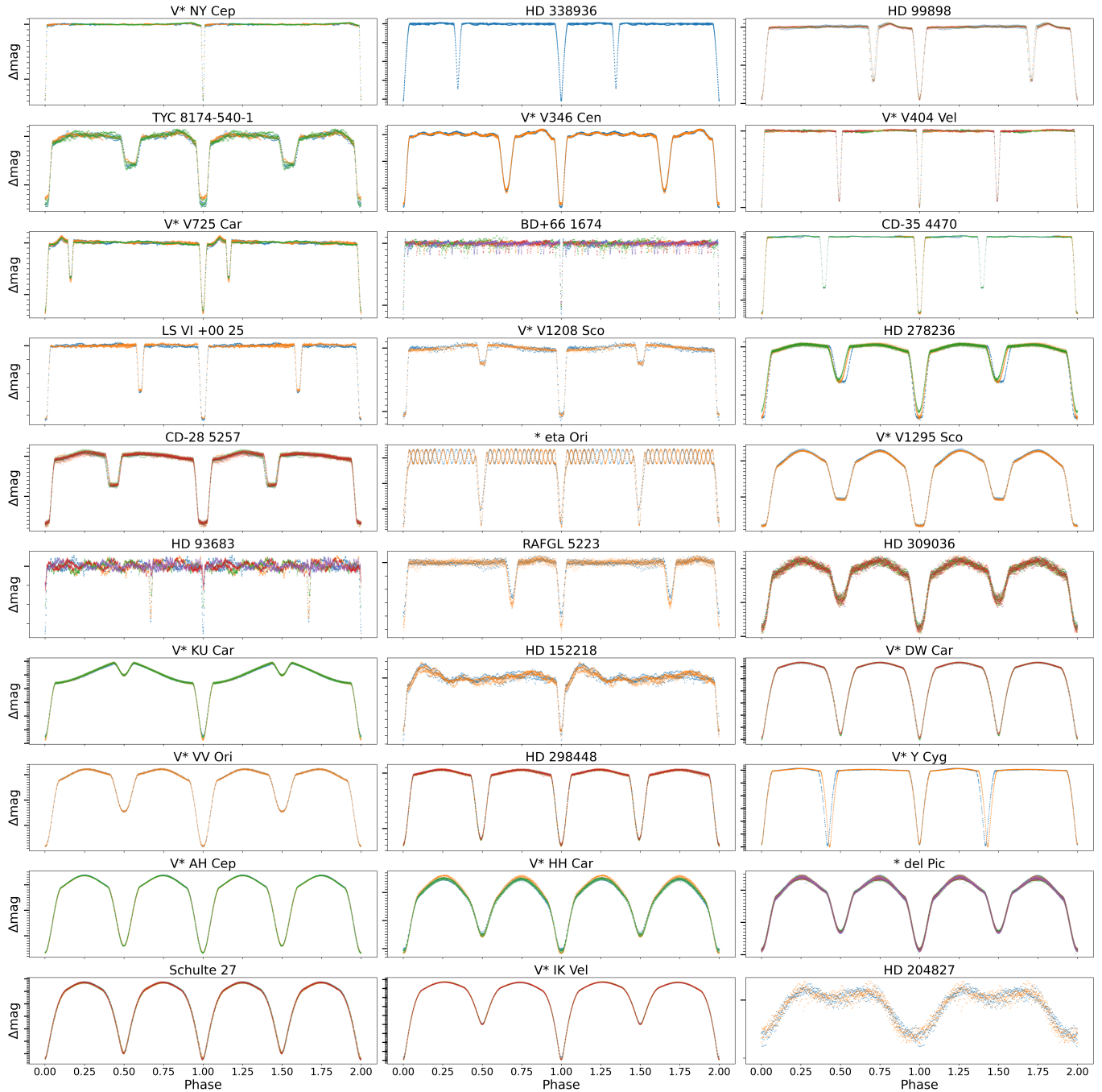


Fig. A.1. Light curves belonging to the confirmed category. In each subplot, bold, long ticks on the Y-axis denote increments of $0.1\Delta\text{mag}$, and thin, short ticks indicate increments of $0.01\Delta\text{mag}$.

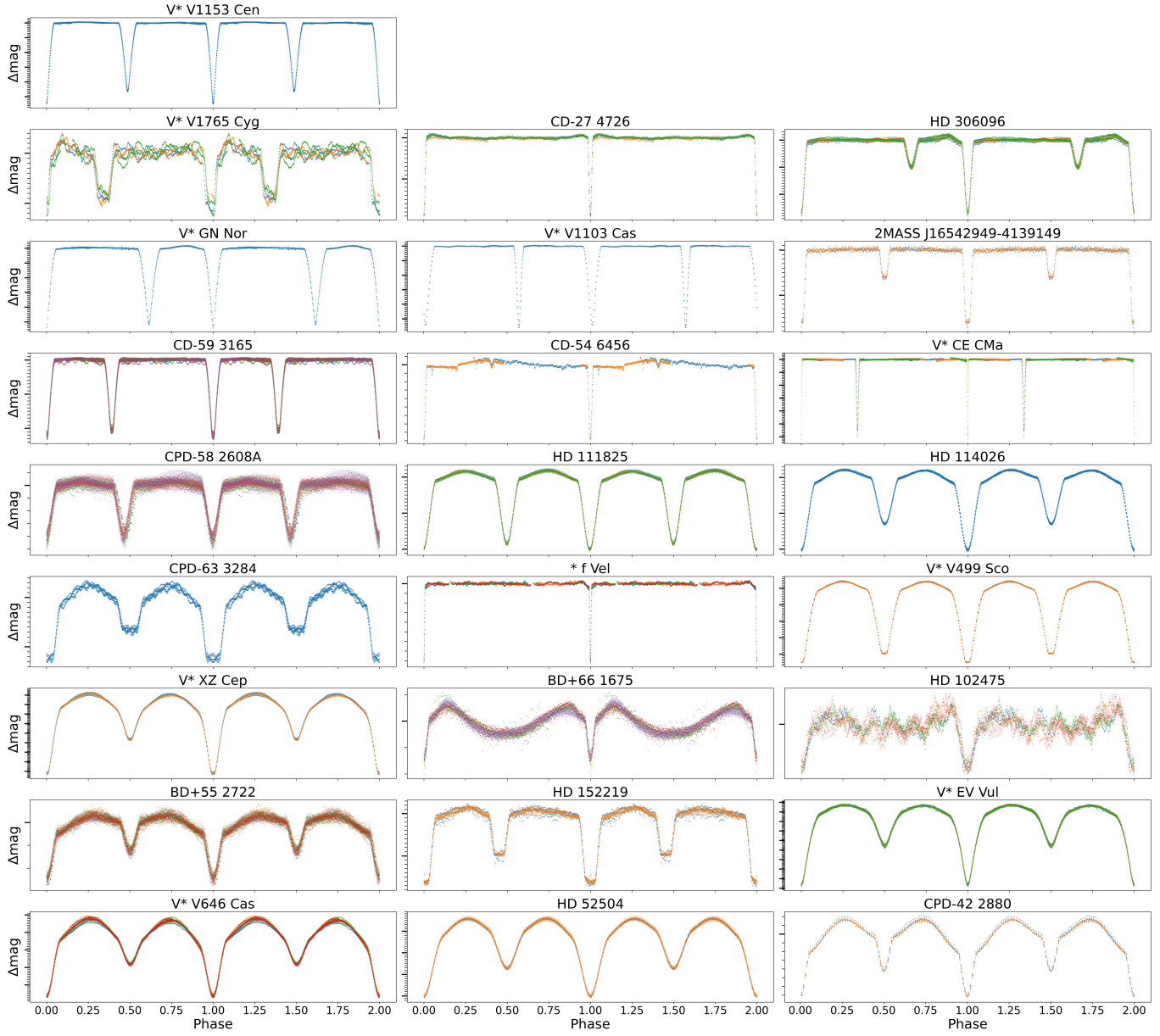


Fig. A.2. Light curves belonging to the candidate category. In each subpanel, bold, long ticks on the Y-axis denote increments of $0.1\Delta mag$, and thin, short ticks indicate increments of $0.01\Delta mag$.

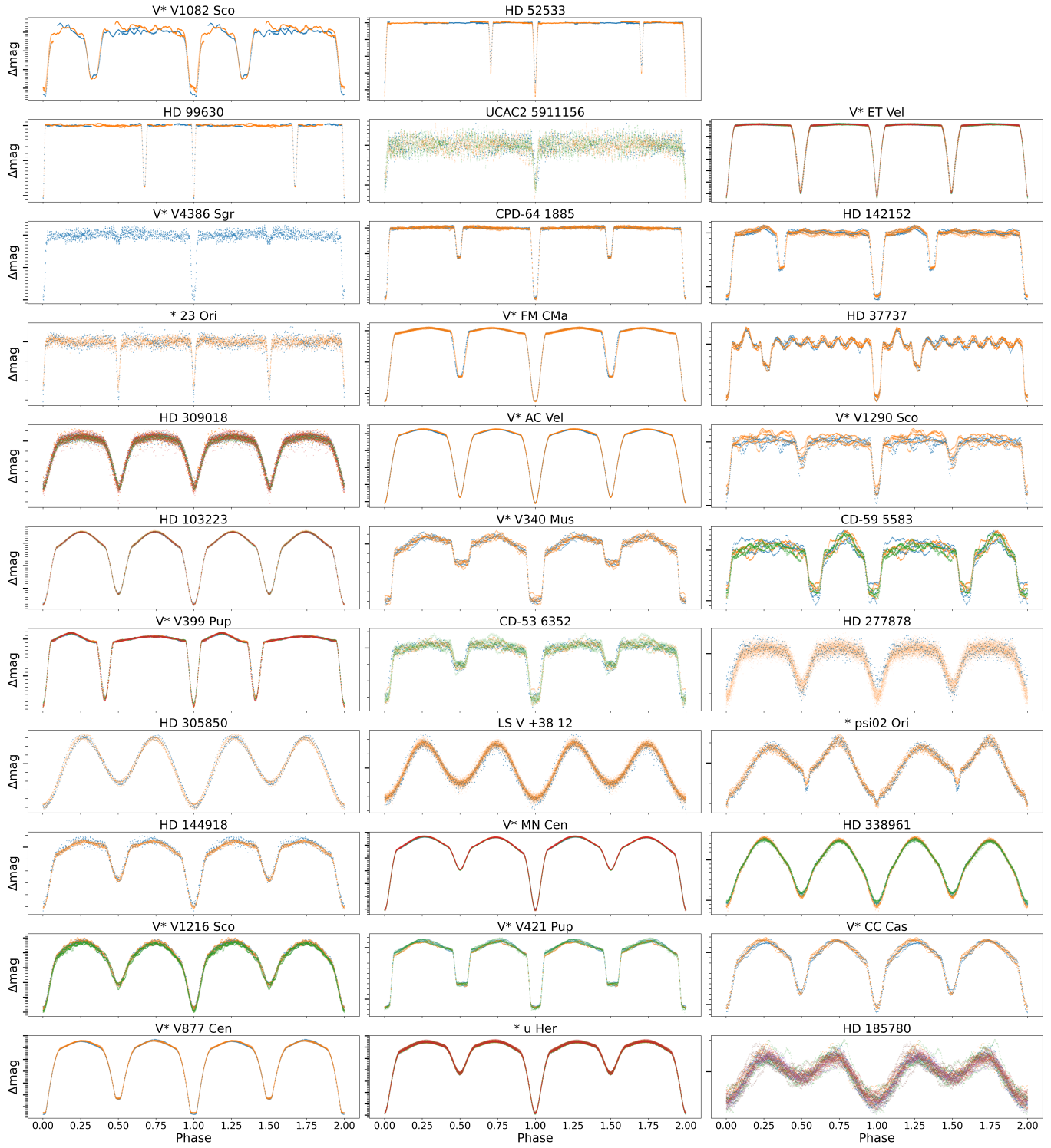


Fig. A.3. Light curves belonging to the unqualified category. In each subpanel, bold, long ticks on the Y-axis denote increments of $0.1\Delta\text{mag}$, and thin, short ticks indicate increments of $0.01\Delta\text{mag}$.